

## A SEMI-ANALYTICAL DESCRIPTION FOR THE FORMATION AND GRAVITATIONAL EVOLUTION OF PROTOPLANETARY DISKS

SANEMICHI Z. TAKAHASHI<sup>1,2</sup>, SHU-ICHIRO INUTSUKA<sup>1</sup>, AND MASAHIRO N. MACHIDA<sup>3</sup>

## ABSTRACT

We investigate the formation process of self-gravitating protoplanetary disks in unmagnetized molecular clouds. The angular momentum is redistributed by the action of gravitational torques in the massive disk during its early formation. We develop a simplified one-dimensional accretion disk model that takes into account the infall of gas from the envelope onto the disk and the transfer of angular momentum in the disk with an effective viscosity. First we evaluate the gas accretion rate from the cloud core onto the disk by approximately estimating the effects of gas pressure and gravity acting on the cloud core. We formulate the effective viscosity as a function of the Toomre  $Q$  parameter that measures the local gravitational stability of the rotating thin disk. We use a function for viscosity that changes sensitively with  $Q$  when the disk is gravitationally unstable. We find a strong self-regulation mechanism in the disk evolution. During the formation stage of protoplanetary disks, the evolution of the surface density does not depend on the other details of the modeling of effective viscosity, such as the prefactor of the viscosity coefficient. Next, to verify our model, we compare the time evolution of the disk calculated with our formulation with that of three-dimensional hydrodynamical simulations. The structures of the resultant disks from the one-dimensional accretion disk model agree well with those of the three-dimensional simulations. Our model is a useful tool for the further modeling of chemistry, radiative transfer, and planet formation in protoplanetary disks.

*Keywords:* accretion, accretion disks — stars: formation

## 1. INTRODUCTION

Since planets are expected to form in protoplanetary disks, planet-formation scenarios should depend on the structure of protoplanetary disks formed through realistic star formation processes. Recent observations have revealed the planets in wide orbits of more than 30 AU (Kalas et al. 2008; Marois et al. 2008; Thalmann et al. 2009). The most convincing scenario to form such planets is the fragmentation of disks due to gravitational instability (Stamatellos et al. 2007; Dodson-Robinson et al. 2009; Vorobyov & Basu 2010; Machida et al. 2010). To investigate the gravitational instability of protoplanetary disks, we need the temperature and density structure of disks. These disk properties can be obtained by revealing the formation process of protoplanetary disks. Cassen & Moosman (1981) have done pioneering theoretical work on the formation and evolution of protoplanetary disks. They calculated the gravitational collapse of a cloud core during the formation of a protoplanetary disk in which they treated the viscosity coefficient of the disk as a parameter. Their modeling was done before more realistic three-dimensional simulations became available.

Recent three-dimensional non-ideal MHD numerical simulations suggest that protoplanetary disks are gravitationally unstable in their early formation stages

because the masses of the disks remain very large (Inutsuka et al. 2010; Machida et al. 2010, 2011a). Massive disks are also formed with non-MHD thin-disk calculations (e.g., Vorobyov & Basu 2006; Vorobyov 2011). In such disks, spiral arms are formed in the case that  $1 \lesssim Q \lesssim 2$ , where  $Q \equiv \kappa c_s / \pi G \Sigma$  is Toomre's parameter,  $\kappa$  is the epicyclic frequency,  $c_s$  is the sound speed,  $G$  is the gravitational constant, and  $\Sigma$  is the surface density of the disk. The angular momentum in disks is redistributed by the action of gravitational torques due to spiral arms. There are some effective viscosity models to mimic the angular momentum transfer due to gravitational torque. An  $\alpha$ -prescription (Shakura & Sunyaev 1973) is used for the effective viscosity models,  $\nu_{\text{eff}} = \alpha c_s^2 / \Omega$ , where  $\Omega$  is the angular frequency of a disk,  $\nu_{\text{eff}}$  is the effective viscosity, and  $\alpha$  is a non-dimensional parameter. Lin & Pringle (1987) and Kratter et al. (2008) investigated the functional forms of  $\alpha$  during disk evolution. Nakamoto & Nakagawa (1994, 1995) and Zhu et al. (2010) performed one-dimensional numerical simulations on the formation of protoplanetary disks from the collapse of a cloud cores using an effective viscosity. Various effective viscosity models were also used in numerical simulations of massive star formation (Yorke & Sonnhalter 2002; Hosokawa et al. 2012). These are axisymmetric two-dimensional simulations using an effective viscosity in place of time-consuming three-dimensional simulations. However, an effective viscosity model that can mimic angular momentum transfer due to gravitational torque is still unknown. Vorobyov (2010) calculated the formation of protoplanetary disks using the effective viscosity models suggested in Lin & Pringle (1987) and Kratter et al. (2008), and compared the resultant disks and protostars with the results of two-dimensional numerical simulations. He con-

<sup>1</sup>Department of Physics, Nagoya University, Furocho, Chikusa-ku, Nagoya, Aichi, 464-8602, Japan; takahashi.sanemichi@a.mbox.nagoya-u.ac.jp, inutsuka@nagoya-u.jp

<sup>2</sup>Department of Physics, Kyoto University, Oiwakecho, Kitashirakawa, Sakyo-ku, Kyoto 606-8502, Japan; sanemichi@tap.scphys.kyoto-u.ac.jp

<sup>3</sup>Department of Earth and Planetary Science, Kyushu University, Higashi-ku, Fukuoka 812-8581, Japan; machida.masahiro.018@m.kyushu-u.ac.jp

cluded that both models cannot mimic the gravitational torque. Thus, further investigation is needed to construct a realistic effective viscosity model, especially when the disk is sufficiently massive to be gravitationally unstable.

In this work, we perform both one-dimensional numerical calculations and three-dimensional numerical simulations. We model the accretion disks using effective viscosity models in the one-dimensional calculation and calculate the formation and evolution of protoplanetary disks in the simulations. Using our results we construct effective viscosity models that can mimic the gravitational torques in the three-dimensional simulations. We also investigate the properties of the resultant disks using our one-dimensional calculations with a wide range of parameters.

We describe our one-dimensional model that incorporates effective viscosity and gas infall from the cloud core in Section 2. In Section 3, we investigate the resultant disks of our calculations. In Section 4, we describe our three-dimensional numerical simulation and show the comparison of the effective viscosity models with the three-dimensional simulations. In Section 5, we discuss the properties of the resultant disks. We summarize our main conclusions in Section 6.

## 2. BASIC EQUATIONS AND SETTINGS FOR ONE-DIMENSIONAL ACCRETION DISK MODEL

### 2.1. Initial Conditions and Accretion onto Disk

Recent observations suggest that the density structures of some prestellar molecular cloud cores can be approximated by Bonnor-Ebert spheres (e.g., Alves et al. 2001). As an initial state, we adopt a Bonnor-Ebert density profile (Ebert 1955; Bonnor 1956) with central density  $3 \times 10^5 \text{ cm}^{-3}$ , radius 17400AU and temperature 10K. We increase the density by a factor of  $f = 1.4$  to promote gravitational collapse. The resultant cloud mass is  $2.5M_{\odot}$ . The cloud core is initially in uniform rotation with angular frequency  $\Omega_0 = 4.8 \times 10^{-14} \text{ s}^{-1}$ . To investigate the cloud evolution, the ratios of thermal and rotational energy to the gravitational energy of the initial cloud are useful and have been used in many previous studies (Tsuribe & Inutsuka 1999; Matsumoto & Hanawa 2003; Machida et al. 2010). The parameters  $f$  and  $\Omega_0$  are related to them as

$$\frac{U}{|W|} = 0.7f^{-1}, \quad (1)$$

$$\frac{T}{|W|} = 1.2 \times 10^{-2} f^{-1} \left( \frac{\Omega_0}{4.8 \times 10^{-14} \text{ s}^{-1}} \right)^2, \quad (2)$$

where  $W$  is gravitational energy,  $U$  is thermal energy, and  $T$  is kinetic energy in the initial core. Note that these parameters are not constants in the time evolution.

Previous studies adopted the density of cloud cores as  $\rho \propto r^{-2}$  (e.g., Cassen & Moosman 1981). In this case, the mass accretion rate onto the disk is constant (Shu 1977). In our work, a Bonnor-Ebert density profile is adopted as an initial condition so that we have to model the mass accretion rate from Bonnor-Ebert spheres, which depend on time. We divide the cloud core into spherical shells of thickness  $\Delta r$  and consider the collapsing motion of each shell (Figure 1). From the

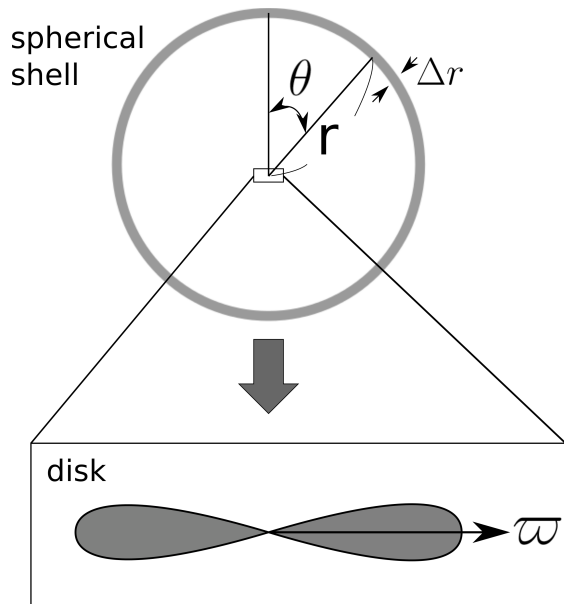


**Figure 1.** Schematic picture for spherical shell and disk formed at the center, where  $r$  is the radius from the center of the cloud core,  $\theta$  is the angle between the initial position of the gas and the rotation axis,  $\Delta r$  is the thickness of the spherical shell, and  $\varpi$  is the radial coordinate of the disk.

equation of motion, the velocity of the shells,  $u$ , obeys the following equation of motion:

$$\begin{aligned} \frac{Du}{Dt} &= -\frac{c_s^2}{\rho} \frac{\partial \rho}{\partial r} - \frac{GM_{\text{in}}}{r^2} \\ &= \frac{c_s^2}{r} F(r) - \frac{GM_{\text{in}}}{r^2}, \end{aligned} \quad (3)$$

where  $r$  is the radius from the center of the cloud core,  $M_{\text{in}}$  is the total mass within the shell, and  $c_s$  is the sound speed of the shell. The total mass within the shell is constant during the collapse as  $M_{\text{in}} = M_{r_{\text{ini}}}$ , where  $r_{\text{ini}}$  is the initial radius of the shell and  $M_{r_{\text{ini}}}$  is the total mass initially contained within the radius  $r_{\text{ini}}$ . Since the envelope is isothermal with  $T = 10\text{K}$ , the sound speed is constant in the envelope. The function  $F(r) = (r/\rho)\partial\rho/\partial r$  depends on the density profile and its value is expected to be of order unity. Since the collapsing shells spend most of their time at outer radii, we approximate  $F(r)$  at the initial radius as  $F(r) = F(r_{\text{ini}}) = \text{const}$ . The initial pressure is equal to the initial gravity before the mass is enhanced by factor  $f$ ,

$$F(r_{\text{ini}}) = \frac{GM_{r_{\text{ini}}}}{fc_s^2 r_{\text{ini}}}. \quad (4)$$

From this approximation, the time in which the gas accretes from the cloud onto the disk is expressed as

$$t_{\text{infall}} = \sqrt{\frac{r_{\text{ini}}}{2GM_{r_{\text{ini}}}}} \int_0^1 \frac{dR}{\sqrt{\frac{1}{f} \ln R + \frac{1}{R} - 1}}. \quad (5)$$

Equation (5) indicates that  $r_{\text{ini}}$  is a function of  $t_{\text{infall}}$  as  $r_{\text{ini}} = r_{\text{ini}}(t_{\text{infall}})$ . Therefore, the initial radius of the shell that accretes onto the disk at time  $t$  is given by  $r_{\text{ini}}(t)$ . The thickness of the shell accreting onto the disk per unit time is given by  $dr_{\text{ini}}/dt$ .

We assume that a spherical shell of the cloud core accretes onto the disk almost simultaneously, and that angular momentum is conserved throughout this process since axial symmetry is almost preserved. This assumption is justified in three-dimensional simulations without large initial non-axisymmetric perturbations (e.g., Machida et al. 2010). We assume that gas accretes onto the disk region where central gravitational force is balanced by centrifugal force. In other words, the accretion radius is determined by the balance between the gravitational force and centrifugal force. The mass accretion rate onto the disk from the cloud core per unit radius is given by  $\partial \dot{M}_{\varpi, \text{infall}} / \partial \varpi$ , where  $\varpi$  is the radial coordinate of the disk, and  $\dot{M}_{\varpi, \text{infall}}(\varpi, t)$  is the total mass of gas that accretes onto the disk within radius  $\varpi$  per unit time.  $\dot{M}_{\varpi, \text{infall}}(\varpi, t)$  is equal to the total mass of the accreting gas per unit time whose specific angular momentum is smaller than  $j(\varpi)$ , the angular momentum defined by the Kepler frequency at radius  $\varpi$ . In the following, we change the variable of  $\dot{M}_{\varpi, \text{infall}}(\varpi, t)$  to relate the region where gas accretes from the cloud core to the initial position of the gas. We change the variable of  $\dot{M}_{\varpi, \text{infall}}(\varpi, t)$  from  $\varpi$  to  $j(\varpi)$ :

$$\frac{\partial}{\partial \varpi} \dot{M}_{\varpi, \text{infall}}(\varpi, t) = \frac{\partial j}{\partial \varpi} \frac{\partial}{\partial j} \dot{M}_{\varpi, \text{infall}}(j, t). \quad (6)$$

The specific angular momentum of the accreting gas is given by the initial radius of the shell  $r_{\text{ini}}(t)$  and the angle between the initial position of the gas and the rotational axis  $\theta$ ,  $j = (r_{\text{ini}}(t) \sin \theta)^2 \Omega_0$ . Therefore, we change the variable of  $\dot{M}_{\varpi, \text{infall}}(j, t)$  again from  $j$  to  $\theta$ ,

$$\frac{\partial}{\partial j} \dot{M}_{\varpi, \text{infall}}(j, t) = 2 \frac{\partial \theta}{\partial j} \frac{\partial}{\partial \theta} \dot{M}_{\varpi, \text{infall}}(\theta, t), \quad (7)$$

where the factor two comes from the fact that gas accretes on both sides of the disk from angle  $\theta$  and  $\pi - \theta$  (Figure 2).

Let us define the total mass accretion rate onto the disk,  $\dot{M}_{\text{infall}}(t)$ , with the integral of the mass accretion rate per unit angle  $\theta$ ,

$$\begin{aligned} \dot{M}_{\text{infall}} &= 2 \int_0^{\frac{\pi}{2}} \frac{\partial \dot{M}_{\varpi, \text{infall}}}{\partial \theta} d\theta \\ &= 2 \int_0^{\frac{\pi}{2}} 2\pi \rho r_{\text{ini}}^2 \frac{dr_{\text{ini}}}{dt} \sin \theta d\theta \\ &= 4\pi \rho r_{\text{ini}}^2 \frac{dr_{\text{ini}}}{dt}, \end{aligned} \quad (8)$$

where the second line is given by the total mass contained in the spherical shell whose radius is  $r_{\text{ini}}$  and thickness is  $dr_{\text{ini}}/dt$ . Thus we can write

$$\frac{\partial \dot{M}_{\varpi, \text{infall}}}{\partial \theta} = 2\pi \rho r_{\text{ini}}^2 \sin \theta \frac{dr_{\text{ini}}}{dt} = \frac{\sin \theta \dot{M}_{\text{infall}}}{2}. \quad (9)$$

From Equations (6), (7) and (9), we obtain a mass accretion rate of

$$\begin{aligned} \frac{\partial \dot{M}_{\varpi, \text{infall}}}{\partial \varpi} &= 2 \frac{\partial \dot{M}_{\varpi, \text{infall}}}{\partial \theta} \frac{\partial \theta}{\partial j} \frac{\partial j}{\partial \varpi} \\ &= \frac{\dot{M}_{\text{infall}}}{2\Omega_0 r_{\text{ini}}^2} \left(1 - \frac{j}{\Omega_0 r_{\text{ini}}^2}\right)^{-\frac{1}{2}} \frac{\partial j}{\partial \varpi}. \end{aligned} \quad (10)$$

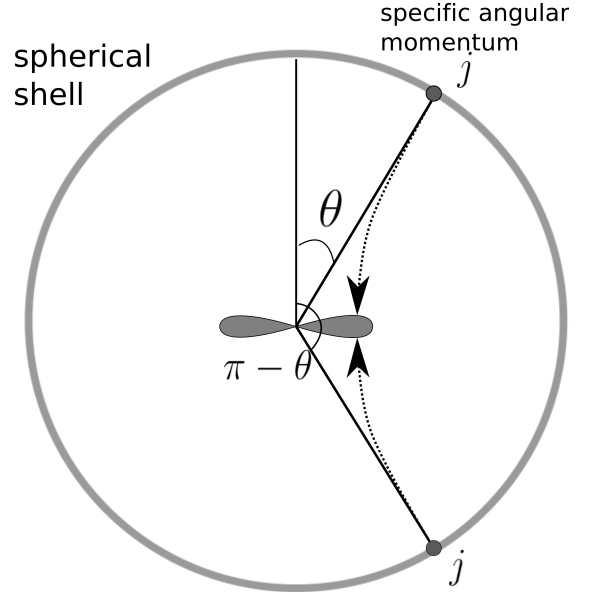


**Figure 2.** Schematic picture of gas accretion from the cloud core. The specific angular momentum of gas with an initial angle  $\theta = \theta_0$  is the same as that with  $\theta = \pi - \theta_0$ . Thus these gases accrete onto the same region of the disk as defined by the centrifugal balance. Note that the actual size of the disk is much smaller than shown in this schematic picture.

## 2.2. The Evolution of Protoplanetary Disks

Using the mass accretion rate given by Equation (10), we derive equations for the evolution of protoplanetary disks (cf. Cassen & Moosman 1981). The angular momentum is mainly redistributed by the action of gravitational torques in the massive disk during its early formation. In this work, we use a simplified one-dimensional accretion disk model that takes into account the infall of gas from the envelope onto the disk and the transfer of angular momentum within the disk in terms of effective viscosity. The surface density evolves according to the mass and angular momentum conservation equations:

$$\frac{\partial}{\partial t} (2\pi \varpi \Sigma) + \frac{\partial F}{\partial \varpi} = \frac{d\dot{M}_{\text{infall}}}{d\varpi}, \quad (11)$$

$$\begin{aligned} \frac{\partial}{\partial t} (2\pi \varpi \Sigma j) + \frac{\partial}{\partial \varpi} (F j) &= \frac{\partial}{\partial \varpi} \left( (2\pi \varpi \Sigma) \nu \varpi^2 \frac{\partial \Omega}{\partial \varpi} \right) \\ &\quad + \frac{d\dot{M}_{\text{infall}}}{d\varpi} j_{\text{acc}}, \end{aligned} \quad (12)$$

where  $\Sigma$  is the surface density,  $F = 2\pi \varpi \Sigma v_{\varpi}$  is the mass flux in the disk (where  $v_{\varpi}$  is the radial velocity of the gas in the disk),  $j$  and  $\Omega$  are the specific angular momentum and angular frequency of the disk, and  $j_{\text{acc}}$  is the specific angular momentum accreting from the cloud core. We ignore the small radial pressure and radial velocity and assume instantaneous centrifugal balance,

$$\frac{j^2}{\varpi^3} = \frac{\partial \Phi}{\partial \varpi}, \quad (13)$$

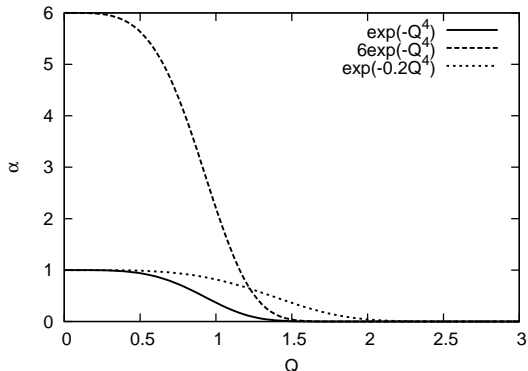


**Figure 3.** Gravitational torque parameter  $\alpha = A \exp(-BQ^4)$  for  $(A, B) = (1, 1)$  (solid line),  $(A, B) = (6, 1)$  (dashed line), and  $(A, B) = (1, 0.2)$  (dotted line).

where  $\Phi$  is the gravitational potential, approximately given by

$$\frac{\partial \Phi}{\partial \varpi} = \frac{GM_{\varpi}}{\varpi^2}, \quad (14)$$

where  $M_{\varpi}$  is the sum of the mass of the central star and the disk mass within  $\varpi$ .<sup>4</sup> The specific angular momentum of the gas accreting from the cloud core is equal to that of the gas in the disk,  $j_{\text{acc}} = j$ .

For the disk viscosity  $\nu$ , we use

$$\nu = \alpha c_s^2 / \Omega \quad (15)$$

(Shakura & Sunyaev 1973). Since gravitational torque is effective only in gravitationally unstable disks,  $\alpha$  is large when the Toomre parameter is  $Q \lesssim 2$ . In this work, and as done by Zhu et al. (2010), we model the gravitational torque parameter as

$$\alpha = A \exp(-BQ^4), \quad (16)$$

where  $A$  and  $B$  are chosen by fitting the results of three-dimensional simulations. The coefficient  $A$  is related to the efficiency of the angular momentum transfer while  $B$  is related to the maximum  $Q$  for which gravitational torque is effective in a gravitationally unstable disk. Figure 3 shows  $\alpha(Q)$  for parameters  $(A, B) = (1, 1)$ ,  $(6, 1)$ ,  $(1, 0.2)$ . The angular momentum in the disk is efficiently redistributed by the action of gravitational torques when  $Q \lesssim 1.5$  for  $(A, B) = (1, 1)$ ,  $(6, 1)$ , and  $Q \lesssim 2$  for  $(A, B) = (1, 0.2)$ . Parameters  $A$  and  $B$  determine how gravitational torque becomes effective. When some region in the disk is gravitationally unstable, spiral arms are formed and propagate into gravitationally stable regions. Then the non-axisymmetric gravitational field and pressure gradients affect the gravitationally stable regions of the disk. Therefore, angular momentum transfer occurs even in gravitationally stable regions if spiral arms appear in the disk. We find that we have to modify the gravitational torque parameter given by Equation (16) as follows:

$$\alpha = \begin{cases} A \exp(-BQ^4) & \text{for } \alpha_{\text{max}} < 0.1, \\ A \exp(-BQ^4) + 0.01 & \text{for } \alpha_{\text{max}} \geq 0.1, \end{cases} \quad (17)$$

<sup>4</sup> We measured the error of this approximation with respect to the numerical calculation of the gravity in thin disk approximation, and found that the difference between our approximate calculation and thin disk approximation was less than 14% at the final snapshot when all of gas accreted on to the disk.

where  $\alpha_{\text{max}}$  is the maximum value of  $\alpha$  in the disk. Note that for the case  $\alpha_{\text{max}} \geq 0.1$  the value of 0.01 is added to better fit the three-dimensional simulations. The validity of this modeling is described in Section 4.

We estimate the sound speed,  $c_s$ , to quantify the viscosity of the  $\alpha$  disk model. To mimic the temperature evolution, we adopt the piecewise polytropic equation of state  $P = \kappa \rho^\gamma$ , where

$$\gamma = \begin{cases} 1 & \text{for } \rho < \rho_{\text{cri}} = 2 \times 10^{-14} \text{g cm}^{-3}, \\ \frac{7}{5} & \text{for } \rho \geq \rho_{\text{cri}}, \end{cases} \quad (18)$$

where  $\kappa = c_{s,10\text{K}}^2 \rho_{\text{cri}}^{1-\gamma}$  and  $c_{s,10\text{K}} = 1.9 \times 10^4 \text{cm s}^{-1}$  (Whitehouse & Bate (2006); Stamatellos & Whitworth (2009); Commerçon et al. (2010); Tomida et al. (2013)). To evaluate the sound speed  $c_s = (\gamma \kappa \rho^{\gamma-1})^{1/2}$  in the disk, we need typical density at a radius  $\varpi$ . When we assume a thin disk,  $z \ll r$ , the equation of hydrostatic equilibrium in the  $z$ -direction is given by

$$\frac{1}{\rho} \frac{\partial P}{\partial z} = -\frac{GM}{\varpi^2} \frac{z}{\varpi}. \quad (19)$$

From this equation, the density profile in the  $z$ -direction is given by

$$\rho = \rho_0 \exp\left(-\frac{z^2}{2H^2}\right), \quad (20)$$

where  $\rho_0$  is the density at the equatorial plane and  $H$  is the scale height,  $H = c_s/\Omega$ . By integrating this equation in the  $z$ -direction, we obtain the disk surface density

$$\Sigma = \sqrt{2\pi} \rho_0 H. \quad (21)$$

Thus the equation for the sound speed at the equatorial plane is

$$\begin{aligned} c_s^2 &= \frac{dP}{d\rho}(z=0) = \gamma \kappa \rho_0^{\gamma-1} \\ &= \gamma \kappa \left( \frac{\Sigma}{\sqrt{2\pi}H} \right)^{\gamma-1} \\ &= \gamma \kappa \left( \frac{\Sigma \Omega}{\sqrt{2\pi}c_s} \right)^{\gamma-1}. \end{aligned} \quad (22)$$

Using the surface density,  $\Sigma$ , and angular frequency,  $\Omega$ , derived in Equations (11) and (12), we can estimate the sound speed as

$$c_s = \left[ \kappa \gamma \left( \frac{\Sigma \Omega}{\sqrt{2\pi}} \right)^{\gamma-1} \right]^{1/(\gamma+1)}. \quad (23)$$

### 2.3. Numerical Procedures

We calculate the formation and evolution of protoplanetary disks using a one-dimensional accretion disk model. We solve Equations (11) and (12) numerically. We start our numerical integration with a protostar mass of  $M_p = 10^{-2} M_\odot$  without a disk. This initial protostellar mass corresponds to the mass of a first core (Masunaga & Inutsuka 2000). The time  $t=0$  is the instant at which a core begins to collapse. We assume a disk radius from 0.1AU to 10000AU in the computational domain. The disk radius is divided into 110 logarithmically equal intervals. (We divide the computational domain into 10 equal intervals from 0.1AU to 1AU and 100

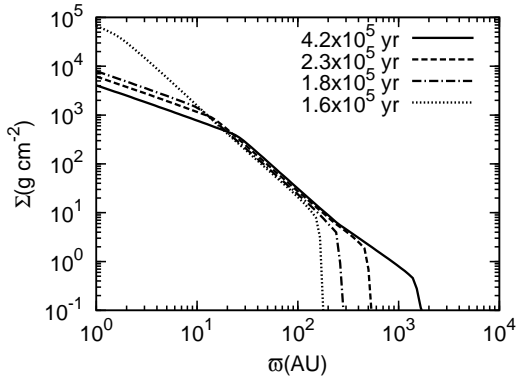


**Figure 4.** Surface density against resultant disk radius  $1.6 \times 10^5$ ,  $1.8 \times 10^5$ ,  $2.3 \times 10^5$ , and  $4.2 \times 10^5$  yr after the cloud core begins to collapse.

logarithmically equal intervals from 1AU to 10000AU.) We assume a zero-torque condition at the center of the disk and zero-flux at the outer boundary. We assume that the gas inside the radius 0.1AU accretes onto the protostar. We neglect the region of the disk from 0.1AU to 1AU because this region weakly depends on the inner boundary condition. We confirmed that an extension of the size of the computational domain or an increase of the size and number of grids do not significantly affect the disk evolution in the region from 1AU to 10000AU.

### 3. RESULTS

#### 3.1. Time Evolution and Dependence on Modeling of Effective Viscosity

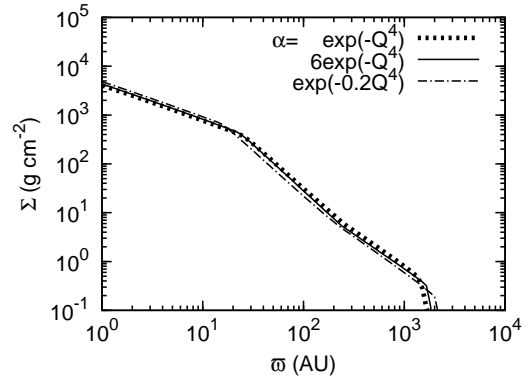
According to the prescription described in Section 2, we calculated the evolution of surface density structures of protoplanetary disks. Figure 4 shows the time evolution of the surface density of the resultant disk with parameters of  $(A, B) = (1, 1)$ . In the early stage of gas infall from the cloud core, infalling gas has a small specific angular momentum since the initial radius of the infalling shell is small. As gas falls onto the disk from outer radii, the disk radius gradually increases. The surface density decreases in the inner region because of viscous diffusion. This tendency is the same as in self-similar solutions of disk evolution (Lynden-Bell & Pringle 1974).

Figure 5 shows the surface density profile after all the gas of the cloud core has accreted onto the disk ( $t = 4.2 \times 10^5$ yr) for three different  $\alpha$  models. There is no significant difference in the surface densities of these models. This suggests that the disk evolution does not depend sensitively on the details of modeling the effective viscosity if the angular momentum in the disk is redistributed by gravitational torques due to gravitational instability.

#### 3.2. Convergence to Self-similar Solution

In this section we discuss the surface density profile of the resultant disk. The disk can be divided into three regions (inner, intermediate, and outer). The surface density distribution in each region converges to the self-similar solution (or static solution), which does not account for the effects of accretion from the cloud core, as explained below.

##### 3.2.1. Inner Region ( $\varpi \lesssim 20$ AU)



**Figure 5.** Surface density after all the gas of the cloud core has accreted onto the disk ( $t = 4.2 \times 10^5$ yr) for parameters  $(A, B) = (1, 1)$ ,  $(A, B) = (6, 1)$ , and  $(A, B) = (1, 0.2)$ .

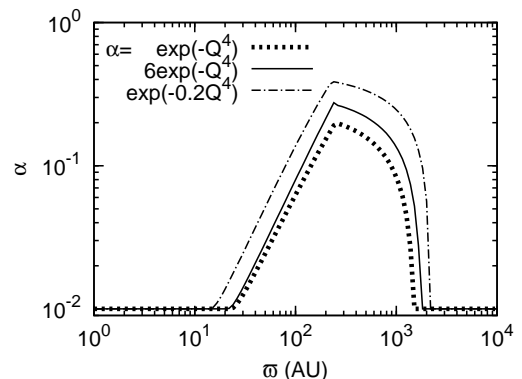


**Figure 6.** Distribution of the viscous parameter  $\alpha$  after all the gas of the cloud core has accreted onto the disk ( $t = 4.2 \times 10^5$ yr) for parameters  $(A, B) = (1, 1)$ ,  $(A, B) = (6, 1)$ , and  $(A, B) = (1, 0.2)$ . The parameter  $\alpha$  is approximately constant ( $\alpha \simeq 0.01$ ) in the region  $\varpi \lesssim 20$ AU.

In the inner region ( $\varpi \lesssim 20$ AU), the disk tends to remain gravitationally stable with no magnetic field (with magnetic field, this region may be gravitationally unstable; see Machida et al. 2011b). In this region, angular momentum is redistributed by the action of non-axisymmetric gravity that is caused by spiral arms formed in other regions. In the inner region, angular frequency and surface density tend to have large values because this region is close to the central star. From Equation (23), the sound speed is also large, because the density is larger than the critical density (Equation (18)). As a result,  $Q$  is much larger than unity and we have  $\alpha = 0.01$ . Figure 6 shows the distribution of the viscous parameter  $\alpha$  at  $t = 4.2 \times 10^5$  yr after all the gas of the cloud core has accreted onto the disk. The parameter  $\alpha$  is approximately constant ( $\alpha \simeq 0.01$ ) in  $\varpi \lesssim 20$ AU.

Since we adopt a polytropic index of  $\gamma = 7/5$  in the inner region, the viscosity,  $\nu$ , is described as

$$\begin{aligned} \nu &= \alpha c_s^2 / \Omega \\ &= \frac{0.01}{\Omega} \left[ \frac{7}{5} \kappa \left( \frac{\Sigma \Omega}{\sqrt{2\pi}} \right)^{\frac{2}{5}} \right]^{\frac{5}{6}} \\ &\propto \Omega^{-2/3} \Sigma^{1/3}. \end{aligned} \quad (24)$$

Suppose that angular frequency is given by Keplerian

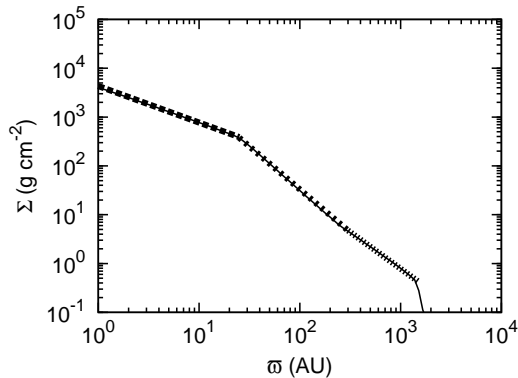


**Figure 7.** Surface density (solid line) derived with parameters  $(A, B) = (1, 1)$ . The self-similar solution (dotted line) is also plotted. Our numerical result is in good agreement with the self-similar solution. The surface density can be fitted by  $\Sigma \propto \varpi^{-3/4}$  ( $\varpi \lesssim 20$  AU),  $\Sigma \propto \varpi^{-1.76}$  ( $20$  AU  $\lesssim \varpi \lesssim 300$  AU), and  $\Sigma \propto \varpi^{-3/2}$  ( $\varpi \gtrsim 300$  AU), respectively.

rotation  $\Omega = \sqrt{GM_{\varpi}/\varpi^3} \propto \varpi^{-3/2}$ . Then Equation (24) is rewritten as

$$\nu \propto \varpi \Sigma^{1/3}. \quad (25)$$

When the surface density shows a convergence to the self-similar solution (Lynden-Bell & Pringle 1974), the surface density distribution is given by

$$\Sigma \propto \frac{\Omega}{\nu \varpi \frac{d\Omega}{d\varpi}} \propto \frac{1}{\nu}. \quad (26)$$

From Equations (25) and (26), we obtain the surface density distribution analytically:

$$\Sigma \propto \varpi^{-3/4}. \quad (27)$$

Figure 7 shows the surface density distribution with parameters  $(A, B) = (1, 1)$  and the analytic solution of  $\Sigma \propto \varpi^{-3/4}$  that fits the numerical result. The figure indicates good agreement between the numerical calculation and self-similar solution in the region  $\varpi \lesssim 20$  AU.

### 3.2.2. Intermediate Region ( $20\text{AU} \lesssim \varpi \lesssim 300\text{AU}$ )

In the intermediate region ( $20\text{AU} \lesssim \varpi \lesssim 300\text{AU}$ ) the disk is gravitationally unstable ( $Q \lesssim 2$ ) owing to a smaller angular frequency,  $\Omega$ , and sound speed,  $c_s$ . Thus  $\alpha$  is larger than 0.01 (Equation (17)). The gas still behaves adiabatically in this region. Figure 8 shows the relation between the parameters  $\alpha$  and  $Q$  for the resultant disk after all of the gas has accreted onto the disk. In this region, the parameter  $\alpha$  is related to  $Q$  by  $\alpha \propto Q^{-10}$  for any parameters  $(A, B)$ . Since the disk mass within the radius  $\varpi$  in the intermediate region is comparable to the central star mass, we approximate  $\Omega = \sqrt{GM_{\varpi}/\varpi^3} \sim \sqrt{G\Sigma/\varpi}$ . Therefore the viscosity is described by

$$\begin{aligned} \nu &\propto Q^{-10} c_s^2 / \Omega \\ &\propto \Sigma^{5/2} \varpi^{36/7}. \end{aligned} \quad (28)$$

From Equation (26), we get  $\Sigma \propto \varpi^{-1.76}$  which is in good agreement with the result of the numerical calculation (see Figure 7). To derive the surface density profile the relation  $\alpha \propto Q^{-10}$  is adopted. The dependence of the

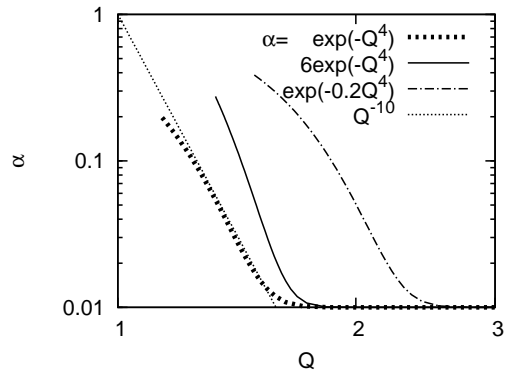


**Figure 8.** Relation between the parameters  $\alpha$  and  $Q$  in the disk after all of the gas has accreted onto the disk. The parameter  $\alpha$  is roughly proportional to  $Q^{-10}$  where the disk is gravitationally unstable with  $\alpha > 0.01$ .

surface density profile on the relation between  $\alpha$  and  $Q$  is discussed in Section 5.

### 3.2.3. Outer Region ( $\varpi \gtrsim 300\text{AU}$ )

In the outer region ( $\varpi \gtrsim 300\text{AU}$ ), the gas behaves isothermally because of the low surface density. In this region the disk is still gravitationally unstable (see Figure 6) and the Toomre parameter  $Q$  is proportional to  $\Omega/\Sigma$  since the sound speed,  $c_s$ , is constant. From Equation (26) we obtain

$$\Sigma \propto \frac{\Omega}{\alpha}, \quad (29)$$

where  $\alpha$  is a function of  $\Omega/\Sigma$ . This equation indicates that the surface density and the angular frequency have the same radial dependence. In this region, surface density is low such that  $M_{\varpi} \sim \text{const}$ . Therefore  $\Sigma \propto \Omega = \sqrt{GM_{\varpi}/\varpi^3} \sim \sqrt{GM_{\text{tot}}/\varpi^3} \propto \varpi^{-3/2}$ . Since the Toomre parameter  $Q \propto \Omega/\Sigma = \text{const}$ , the radial dependence of the surface density distribution is estimated directly from the definition of  $Q$ ,

$$\begin{aligned} \Sigma &= \frac{\Omega c_s}{\pi G Q} \\ &\sim 1[\text{g cm}^{-2}] \left( \frac{M_{\text{tot}}}{1M_{\odot}} \right)^{1/2} \left( \frac{\varpi}{1000\text{AU}} \right)^{-3/2}. \end{aligned} \quad (30)$$

This surface density distribution shows good agreement with the numerical result (Figure 7).

From our results, the overall surface density distribution of the resultant disk is given by

$$\Sigma \propto \begin{cases} \varpi^{-3/4} & (\varpi \lesssim 20\text{AU}) \\ \varpi^{-1.76} & (20\text{AU} \lesssim \varpi \lesssim 300\text{AU}) \\ \varpi^{-3/2} & (\varpi \gtrsim 300\text{AU}). \end{cases} \quad (31)$$

## 4. COMPARISON WITH 3D SIMULATIONS

### 4.1. Model

To verify the evolution of the protoplanetary disk calculated in Section 3, we compare the resultant disk of our model with that of three-dimensional hydrodynamical simulations, originally performed in Machida et al. (2010).

## 4.1.1. Basic Equations

We solve equation of the mass conservation and the equation of motion including self-gravity:

$$\frac{\partial \rho}{\partial t} + \nabla \cdot (\rho \mathbf{v}) = 0, \quad (33)$$

$$\rho \frac{\partial \mathbf{v}}{\partial t} + \rho (\mathbf{v} \cdot \nabla) \mathbf{v} = -\nabla P - \rho \nabla \phi. \quad (34)$$

The gravitational potential is composed of two parts:

$$\phi = \phi_{\text{gas}} + \phi_{\text{ps}}, \quad (35)$$

$$\nabla^2 \phi_{\text{gas}} = 4\pi G \rho, \quad (36)$$

$$\phi_{\text{ps}} = -\frac{GM_{\text{ps}}}{r}, \quad (37)$$

where the subscript ps refers to protostar quantities. We assume a barotropic gas that mimics the thermal evolution of radiation hydrodynamical simulation (Masunaga & Inutsuka 2000; Tomida et al. 2013),

$$P = c_s^2 \rho + \kappa \rho^\gamma \left[ \tanh \left( \frac{\rho}{\rho_{\text{cri}}} \right) \right]^{\frac{1}{10}}, \quad (38)$$

$$\kappa = c_s^2 \rho_{\text{cri}}^{1-\gamma}, \quad (39)$$

where  $\gamma = 7/5$  and  $\rho_{\text{cri}} = 2 \times 10^{-14} \text{g cm}^{-2}$  are adopted. When  $\rho < \rho_{\text{cri}}$ , the gas is isothermal and the sound speed is  $c_s = 1.9 \times 10^4 \text{cm s}^{-1}$ . When  $\rho > \rho_{\text{cri}}$ , the gas is adiabatic with  $\gamma = 7/5$ . The initial condition is the same as that given in Section 2, i.e., a Bonner-Ebert sphere whose central density is  $3 \times 10^5 \text{cm}^{-3}$  and radius is 17400AU.

## 4.1.2. Sink Cell

To realize a long-term calculation of the protoplanetary disk, we adopt a sink cell at the center of the disk. When the number density in the region  $r < r_{\text{sink}} = 1\text{AU}$  exceeds  $n_{\text{th}} = 10^{12} \text{cm}^{-3}$ , we assume that the gas accretes onto the protostar, and remove the gas exceeding the threshold density  $n_{\text{th}}$  from the computational domain and add it to the protostellar mass. We confirmed that the calculation results do not significantly depend on the values of  $r_{\text{sink}}$  and  $n_{\text{th}}$ .

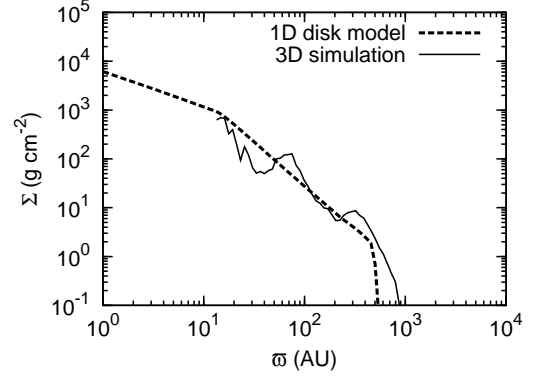
## 4.2. Comparison

Figure 9 shows surface density profiles of the resultant disks from the three-dimensional simulation and one-dimensional accretion disk model. We use  $\alpha = \exp(-Q^4)$  for an effective viscosity model. The surface density distribution for the effective viscosity model is very similar to that of the three-dimensional simulation.

Figure 10 shows the evolution of the protostar and protoplanetary disk masses. The mass evolution of the protostar and protoplanetary disk derived in our effective viscosity model is similar to that of the three-dimensional simulations. These results show that our effective viscosity model may provide a simplified description for the evolution of a gravitationally unstable disk formed through the collapse of molecular a cloud core.

## 5. DISCUSSION

## 5.1. Dependence on Effective Viscosity



**Figure 9.** Surface density profiles of resultant disks from three-dimensional simulation (solid) and one-dimensional accretion disk model (dashed) at  $t = 2.3 \times 10^5 \text{yr}$ . We use  $\alpha = \exp(-Q^4)$  for an effective viscosity model.

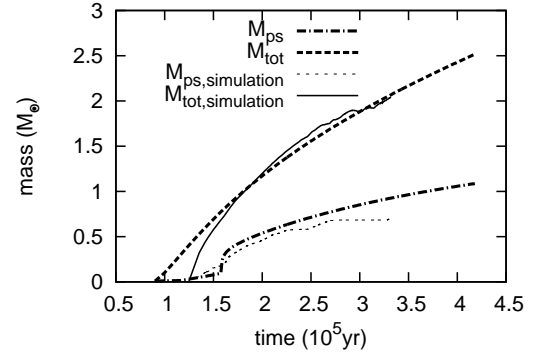


**Figure 10.** Protostar and protoplanetary disk mass as a function of time after the cloud begins to collapse.

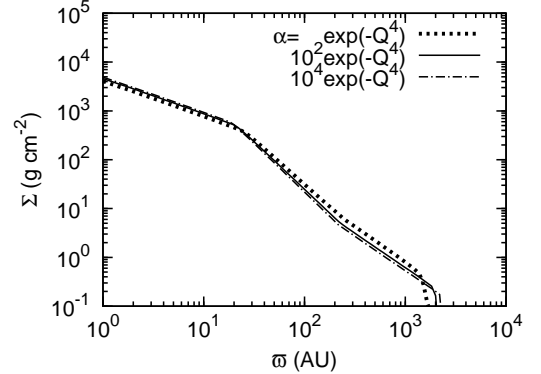


**Figure 11.** Surface density distributions for parameters  $A = 1$  (dotted),  $A = 10^2$  (solid), and  $A = 10^4$  (dash-dotted) as a function of distance from the central star,  $\varpi$ .

In this work angular momentum transfer due to gravitational torques is modeled by  $\alpha = A \exp(-BQ^4)$  in the intermediate and outer disk regions. In Section 3 we found that the resultant disks do not depend on the parameters  $A$  and  $B$  sensitively. We performed numerical calculations for a wide range of  $A$  in order to investigate the dependence on the model parameters.

Figure 11 shows the surface density distributions of the resultant disks for  $A = 1$ ,  $10^2$ , and  $10^4$ . Although  $A$  differs by four orders of magnitude, there is no signifi-

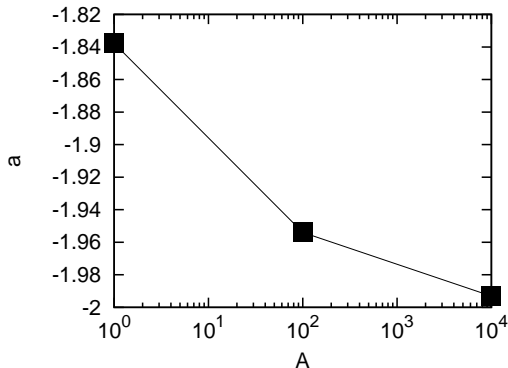


**Figure 12.** Relation between the parameter  $A$  and the slope of the surface density in the intermediate region. The parameter  $a$  is the exponent of surface density  $\Sigma \propto \varpi^a$ .

cant difference among the models. One of the interesting features is the slope of the surface density profile in the intermediate region. Figure 12 shows the relation between parameter  $A$  and the slope of the surface density. Although the slope is steeper for larger  $A$ , its dependence is not so strong. In the case  $\Sigma \propto \varpi^a$  and  $\alpha \propto Q^{-b}$ ,  $a$  is related to  $b$  by

$$a = -\frac{7b + 4}{3b + 12}, \quad (40)$$

in the case that the disk converges to the self-similar solutions. Thus, if  $b$  is large and  $\alpha$  depends sensitively on  $Q$ , the density profiles converge to  $\Sigma \propto \varpi^{-7/3}$ . Here, large  $A$  corresponds to large  $b$ . Therefore, the value of the parameter  $a$  is close to  $-7/3$  when the parameter  $A$  is large as shown in Figure 12.

### 5.2. Relation between $\alpha$ , $Q$ , and $F$

The maximum value of  $\alpha$  due to gravitational torque is still unknown. In our model, the parameter  $A$  is related to the efficiency of the angular momentum transfer through gravitational torques. However, Figures 6 and 8 suggest that the maximum value of  $\alpha$  does not strongly depend on  $A$ . The maximum value of the parameter  $\alpha$  is about 0.2 for all models. This maximum value is not controlled by the parameter  $A$ , but by the mass accretion rate from the cloud core onto the disk. The structure of the disk converges to the self-similar solution, and the mass flux in the disk is similar to the gas accretion rate from the cloud core to the protoplanetary disk. In the case that the mass flux in the disk is less than the gas accretion from the cloud core, gas accumulates on the disk. Therefore, the disk becomes gravitationally unstable;  $Q$  decreases and  $\alpha$  increases. On the other hand, in the case that the mass flux is larger than the gas accretion from the cloud core, the disk mass decreases. Then, the disk becomes gravitationally stable and the mass flux decreases. As a result, the mass flux in the disk has a similar value to the mass accretion rate from the cloud core. Using Equation (11) and (12), the mass flux in the disk is given by

$$F = \frac{1}{\frac{\partial j}{\partial \varpi}} \left[ \frac{\partial}{\partial \varpi} \left( 2\pi \Sigma \nu \varpi^3 \frac{\partial \Omega}{\partial \varpi} \right) - 2\pi \varpi \Sigma \frac{\partial j}{\partial t} \right]. \quad (41)$$

We ignore the second term of Equation (41) because this is smaller than the first term and use the relations  $\Omega \propto$

$\varpi^{-1.5}$  and  $\Sigma \propto \varpi^{-1.5}$  for simplicity. Using Equation (15) and Toomre's  $Q$  parameter, we can rewrite Equation (41) as

$$F \simeq -3 \left( \frac{c_s^2}{v_\phi^2} \right)^{3/2} G^{1/2} M_\varpi^{3/2} \varpi^{-3/2} \frac{\alpha}{Q}. \quad (42)$$

Using a typical mass accretion rate from the cloud core, Equation (42) is given by  $F \sim c_s^3/G \sim 2 \times 10^{-6} M_\odot \text{ yr}^{-1}$ , such that

$$\alpha \simeq 0.2Q \left( \frac{F}{2 \times 10^{-6} M_\odot \text{ yr}^{-1}} \right) \left( \frac{v_\phi^2/c_s^2}{100} \right)^{3/2} \times \left( \frac{r}{300 \text{ AU}} \right)^{3/2} \left( \frac{M_r}{1 M_\odot} \right)^{-3/2}. \quad (43)$$

Therefore we obtain  $\alpha = 0.2Q$  at  $\varpi = 300 \text{ AU}$  at which  $\alpha$  has its largest value in the disk (Figure 6). Figure 13 shows the function  $\alpha = 0.2Q$  and also shows the relations between  $\alpha$  and  $Q$  after all of the gas of the cloud core accretes onto the disk ( $t = 4.2 \times 10^5 \text{ yr}$ ) for different values of the parameters ( $A$ ,  $B$ ). Equation (43) can roughly estimate the value of  $\alpha$  at 300 AU. If we know where the value of  $\alpha$  is largest, Equation (43) gives the maximum  $\alpha$ . Thus, the maximum  $\alpha$  is related to the gas accretion rate from the cloud core, not the parameter  $A$ . In other words, the parameter  $\alpha$  changes only slightly even if the functional form of the effective  $\alpha$  changes drastically. Even if we change the parameter  $A$  by four orders of magnitude, the difference between parameters  $\alpha$  and  $Q$  is less than factor three (Figure 13). This is because we use the effective viscosity model in which  $\alpha$  changes drastically when  $Q$  changes slightly. When model parameters for viscosity, such as  $A$ , are changed, the mass flux in the disk balances the mass accretion rate from the cloud core by changing the surface density  $\Sigma$  slightly. Therefore, the structure of the disk is self-regulated to achieve the balance between the mass flux in the disk and the mass accretion rate from the cloud core. Thus, the surface density of the resultant disk does not depend on the details of the modeling of effective viscosity.

### 5.3. Dependence on Initial Condition

We have shown the resultant disk formed from a cloud core appropriated by a Bonner-Ebert sphere with mass  $2.5 M_\odot$ , angular frequency  $\Omega_0 = 4.8 \times 10^{-14} \text{ s}^{-1}$ , and mass enhancement factor  $f = 1.4$ . Now we change the parameters of the cloud core, and discuss the dependence of the resultant disk on the initial conditions.

#### 5.3.1. Angular Momentum of Cloud Cores

It remains difficult to observe the angular momentum of a cloud core. However, the angular momentum of the accreting gas depends on that of the cloud core, which determines the radius at which the gas accretes. Thus, the initial angular momentum of the cloud core plays an important role in the formation of protoplanetary disks. To investigate the effects of initial angular momentum, we performed a number of calculations of protoplanetary disk formation with cloud cores of different angular frequencies. The surface density distributions of the resultant disks are shown in Figure 14. Since gas accretes onto the region where the gravitational force is balanced

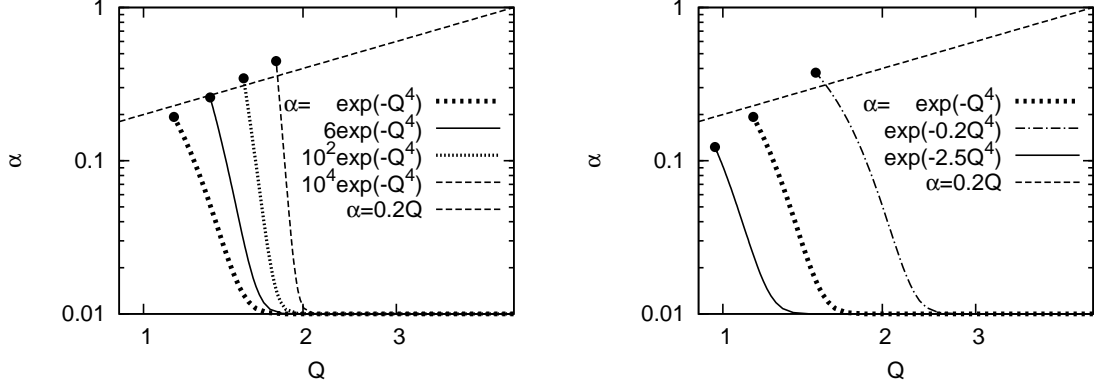


**Figure 13.** Relation between  $\alpha$  and  $Q$ . The dotted line shows  $\alpha = 0.2Q$  as given by Equation (43). Filled circles show  $\alpha$  and  $Q$  at  $\varpi = 300$  AU. Equation (43) can roughly estimate the value of  $\alpha$  at 300AU.

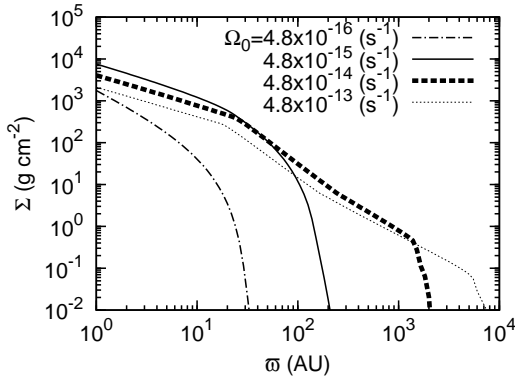


**Figure 14.** Surface density distributions of the resultant disks for  $\Omega_0 = 4.8 \times 10^{-16}$ ,  $4.8 \times 10^{-15}$ ,  $4.8 \times 10^{-14}$ ,  $4.8 \times 10^{-13} \text{ s}^{-1}$  after all of the gas of the cloud core has accreted onto the disk.

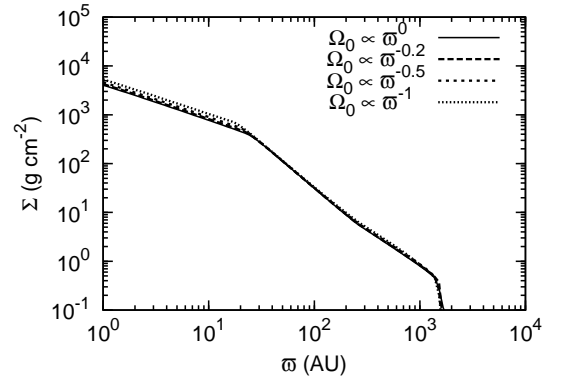


**Figure 15.** Surface density distributions of the resultant disks for various initial rotation profiles,  $\Omega_0 \propto \varpi^0$ ,  $\varpi^{-0.2}$ ,  $\varpi^{-0.5}$ ,  $\varpi^{-1}$  just after all of the gas in the cloud core accrete onto the disk. Total angular momentum of the cloud cores are the same as that of our fiducial model with  $\Omega_0 = 4.8 \times 10^{-14} \text{ s}^{-1}$ .

by the centrifugal force, gas accretes onto the outer region of the disk when the angular frequency of the cloud core is sufficiently large. Thus, such a core forms larger disk.

The initial angular momentum of a cloud core does not affect the mass accretion rate onto a disk (Equation (8)). As discussed above, the order of the mass flux in the disk is the same as the order of the mass accretion rate from the cloud core to the disk,  $\sim 10^{-6} M_\odot \text{ yr}^{-1}$ . The mass flux in the disk depends heavily on the surface density through the  $\alpha$  parameter. Thus, the fact that mass flux does not depend on the angular momentum of the cloud core means that the value of the surface density does not depend sensitively on the angular momentum of the cloud core.

So far a rigidly rotating cloud core is used as the initial condition for our fiducial models. The rotation laws of the actual star-forming dense cores in molecular clouds are unknown observationally. Thus, in the following we investigate how the result depends on the initial rotation profile, by comparing the surface density structures of the resultant disks formed from cloud cores with various rotation profile,  $\Omega_0 \propto \varpi^0$ ,  $\varpi^{-0.2}$ ,  $\varpi^{-0.5}$ ,  $\varpi^{-1}$ , where  $\varpi$  is a distance from a rotation axis. These cores have the same total angular momentum. Since gas accretes onto the disk region where central gravitational force is balanced by centrifugal force, angular momentum distributions of the cloud cores are affect the region where

gas accretes from the cloud cores. Differentially rotating cores ( $\Omega_0 \propto \varpi^{-0.2}$ ,  $\varpi^{-0.5}$ ,  $\varpi^{-1}$ ) have larger angular momenta in the inner part and smaller angular momenta in the outer part than the rigidly rotating core. Therefore disks formed from the differentially rotating cores have larger angular momenta than that of rigidly rotating core in the early phase of accretion. At the end of the accretion, gas with smaller angular momentum accretes onto the disk from differentially rotating cores than in the rigidly rotating core.

Figure 15 shows the density distributions of the resultant disks after all the gas in the cloud core accrete onto the disk. Although the initial angular momentum distributions are different, the surface density distributions of resultant disks are similar to that from rigidly rotating core. Since angular momentum of the disk is well redistributed by the gravitational torque, the difference in the initial angular momentum distribution of the cloud core produces only a small effect on the resultant disk.

### 5.3.2. Mass Accretion Rate from the Cloud Core onto the Disk

The mass accretion rate from the cloud core onto the disk depends on the properties of the cloud core. Therefore the formation process of the cloud core should determine the properties of the cloud core. In our fiducial model, we increased the density of the Bonnor-

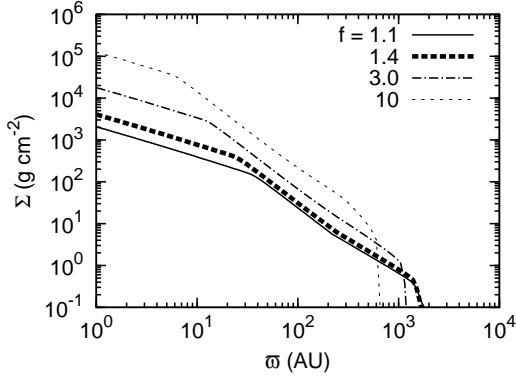


**Figure 16.** Surface density distributions of the resultant disks for  $\Omega_0 = 4.8 \times 10^{-14} \text{s}^{-1}$  and  $f = 1.1, 1.4, 3, 10$  after all of the gas of the cloud core has accreted onto the disk.

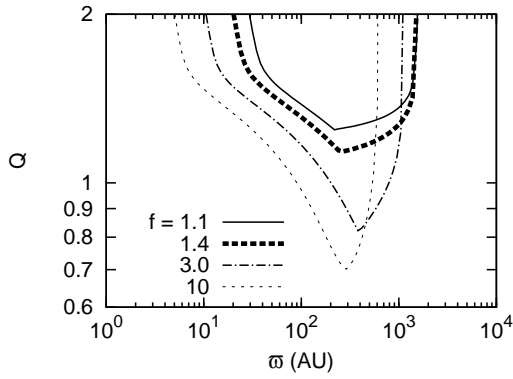


**Figure 17.** Distributions of  $Q$  of the resultant disks for  $\Omega_0 = 4.8 \times 10^{-14} \text{s}^{-1}$  and  $f = 1.1, 1.4, 3, 10$  after all of the gas of the cloud core has accreted onto the disk.

Ebert spheres by a factor of  $f = 1.4$ , corresponding to  $U/|W| = 0.5$ , in order to promote gravitational collapse. We can change the mass accretion rate onto the disk by changing  $f$ . A large value of  $f$  (this means small  $U/|W|$ ) corresponds to a large mass accretion rate onto the disk. We performed numerical calculations with  $f = 1.1, 1.4, 3, 10$  ( $U/|W| = 0.64, 0.5, 0.23, 0.07$ ). Figure 16 shows the density distributions of the resultant disks after all the gas of the cloud core has accreted onto the disk. When we adopt larger  $f$  (or smaller  $U/|W|$ ), both the mass accretion rate onto the disk and the mass flux in the disk are large. As a result, the surface density is large for larger  $f$ . On the other hand, it takes longer time for gas to accrete from a cloud core with smaller  $f$ . At the outer edge of the disk, the angular momentum of the gas increases because angular momentum is transported from the inner part to the outer part. Thus, the disk radius increases over time. Therefore, a larger disk forms when  $f$  is small. Figure 17 shows the distributions of  $Q$  for various  $f$ . For models with  $f > 3$ , the Toomre parameter  $Q$  is smaller than unity at the radius  $\varpi \sim 300 \text{AU}$  ( $Q \simeq 0.8$  for  $f = 3$ ,  $Q \simeq 0.7$  for  $f = 10$ ).

## 6. CONCLUSIONS

In this paper we investigated the formation process of self-gravitating protoplanetary disks. We developed a simplified one-dimensional accretion disk model that accounts for the infall of gas from the envelope onto the

disk. We also modeled the transfer of angular momentum within the disk in terms of an effective viscosity. The resultant disk consist of three regions. The inner region of the disk are adiabatic and gravitationally stable. The intermediate region is also adiabatic but gravitationally unstable. The outer region is isothermal and gravitationally unstable. The structure of the surface density profiles of the disks converge to self-similar solutions. The radial dependence of the disk surface density is described by  $\Sigma \propto \varpi^{-3/4}$  for the inner region,  $\Sigma \propto \varpi^{-1.7} \sim \varpi^{-2}$  for the intermediate region, and  $\Sigma \propto \varpi^{-3/2}$  for the outer region.

We also performed three-dimensional numerical simulations starting from the collapse of cloud cores to the formation of the protoplanetary disks. We compared the three-dimensional simulations with our one-dimensional accretion disk model and confirmed that our model of effective viscosity can provide a simplified description for the evolution of a gravitationally unstable disk.

In addition, we used an effective viscosity model in which  $\alpha$  changes sensitively with  $Q$  when the disk is gravitationally unstable. This model shows a strong self-regulation mechanism in protoplanetary disks.

The structure of the disk depends on the initial state of the cloud core. The disk radii depends on the initial rotation frequency of the cloud core. Massive, gravitationally unstable cloud cores cause a high mass accretion rate onto the disk. In such a cloud, a massive disk forms and becomes gravitationally unstable. In this work,  $Q$  is minimum at  $\varpi \sim 300 \text{AU}$  which is the boundary between the intermediate and outer disk regions. This result suggests that fragmentation of the disk occurs at outer radii  $> 100 \text{AU}$  in accordance with three-dimensional numerical simulations of protostellar collapse (e.g., Machida et al. 2010)

With our effective viscosity model, we are able to calculate protoplanetary disk formation more easily and more rapidly than using three-dimensional simulations. Our model is thus a useful tool for further modeling of chemistry, radiative transfer and planet formation in protoplanetary disks.

We thank Takashi Nakamura and Kazuyuki Omukai for their continuous encouragement and Kohei Inayoshi for fruitful discussion. Data analysis was carried out in part on the Yukawa Institute Computer Facility and the general-purpose PC farm at the Center for Computational Astrophysics, CfCA, of the National Astronomical Observatory of Japan.

## REFERENCES

- Alves, J. F., Lada, C. J., & Lada, E. A. 2001, *Nature*, 409, 159
- Bonnor, W. B. 1956, *MNRAS*, 116, 351
- Cassen, P., & Moosman, A. 1981, *Icarus*, 48, 353
- Commerçon, B., Hennebelle, P., Audit, E., Chabrier, G., & Teyssier, R. 2010, *A&A*, 510, L3
- Dodson-Robinson, S. E., Veras, D., Ford, E. B., & Beichman, C. A. 2009, *ApJ*, 707, 79
- Ebert, R. 1955, *ZAp*, 37, 217
- Hosokawa, T., Yoshida, N., Omukai, K., & Yorke, H. W. 2012, *ApJ*, 760, L37
- Inutsuka, S., Machida, M. N., & Matsumoto, T. 2010, *ApJ*, 718, L58
- Kalas, P., Graham, J. R., Chiang, E., et al. 2008, *Science*, 322, 1345
- Kratter, K. M., Matzner, C. D., & Krumholz, M. R. 2008, *ApJ*, 681, 375
- Lin, D. N. C., & Pringle, J. E. 1987, *MNRAS*, 225, 607
- Lynden-Bell, D., & Pringle, J. E. 1974, *MNRAS*, 168, 603

- Machida, M. N., Inutsuka, S., & Matsumoto, T. 2010, *ApJ*, 724, 1006
- Machida, M. N., Inutsuka, S., & Matsumoto, T. 2011a, *PASJ*, 63, 555
- Machida, M. N., Inutsuka, S., & Matsumoto, T. 2011b, *ApJ*, 729, 42
- Marois, C., Macintosh, B., Barman, T., et al. 2008, *Science*, 322, 1348
- Masunaga, H., & Inutsuka, S. 2000, *ApJ*, 531, 350
- Matsumoto, T., & Hanawa, T. 2003, *ApJ*, 595, 913
- Nakamoto, T., & Nakagawa, Y. 1994, *ApJ*, 421, 640
- Nakamoto, T., & Nakagawa, Y. 1995, *ApJ*, 445, 330
- Shakura, N. I., & Sunyaev, R. A. 1973, *A&A*, 24, 337
- Shu, F. H. 1977, *ApJ*, 214, 488
- Stamatellos, D., Hubber, D. A., & Whitworth, A. P. 2007, *MNRAS*, 382, L30
- Stamatellos, D., & Whitworth, A. P. 2009, *MNRAS*, 400, 1563
- Thalmann, C., Carson, J., Janson, M., et al. 2009, *ApJ*, 707, L123
- Tomida, K., Tomisaka, K., Matsumoto, T., et al. 2013, *ApJ*, 763, 6
- Tsuribe, T., & Inutsuka, S. 1999, *ApJ*, 523, L155
- Vorobyov, E. I. 2010, *New A*, 15, 24
- Vorobyov, E. I. 2011, *ApJ*, 729, 146
- Vorobyov, E. I., & Basu, S. 2006, *ApJ*, 650, 956
- Vorobyov, E. I., & Basu, S. 2010, *ApJ*, 714, L133
- Whitehouse, S. C., & Bate, M. R. 2006, *MNRAS*, 367, 32
- Yorke, H. W., & Sonnhalter, C. 2002, *ApJ*, 569, 846
- Zhu, Z., Hartmann, L., & Gammie, C. 2010, *ApJ*, 713, 1143